PAPER

Bound fermion states in pinned vortices in the surface states of a superconducting topological insulator

IOP Publishing Journal of Physics: Condensed Matter
J. Phys.: Condens. Matter **33** (2021) 035604 (11pp) https://doi.org/10.1088/1361-648X/abba89

Bound fermion states in pinned vortices in the surface states of a superconducting topological insulator

Haoyun Deng[1,2], N Bonesteel[1,2] and P Schlottmann[1,2,*]

[1] Department of Physics, Florida State University, Tallahassee, FL 32306, United States of America
[2] National High Magnetic Field Laboratory, Florida State University, Tallahassee, Florida 32310, United States of America

E-mail: pschlottmann@fsu.edu

Received 19 May 2020, revised 23 August 2020
Accepted for publication 22 September 2020
Published 20 October 2020

Abstract

By analytically solving the Bogoliubov–de Gennes equations we study the fermion bound states at the center of the core of a vortex in a two-dimensional superconductor. The superconducting states are induced via proximity effect between an *s*-wave superconductor and the surface states of a strong topological insulator. The strong spin–orbit coupling locks the spin perpendicular to the momentum (Rashba interaction). A zero-energy Majorana state arises together with an equally spaced (Δ_∞^2/E_F) sequence of fermion excitations. The spin–momentum locking is key to the formation of the Majorana state. We present analytical expressions for the energy spectrum and the wave functions of the bound states. The wave functions fall off exponentially with the distance ρ from the core of the vortex as $\exp[-\int_0^\rho d\rho' \Delta(\rho')/v_F]$. An analytic expression for the local density of states (LDOS) for the bound states is obtained. The particle–hole symmetry is broken in the LDOS as a consequence of the spin–orbit coupling. The spin-polarization of the bound states is discussed. We also obtain the energy shifts of the bound states in a small magnetic field. A unitary transformation relating the model with Rashba interaction to the Dirac Hamiltonian is presented.

Keywords: superconductivity, topological insulator, Majorana, bound states in vortex

(Some figures may appear in colour only in the online journal)

1. Introduction

Majorana fermions are unconventional quantum states with non-abelian statistics and potential for quantum computing [1]. The idea of storing quantum information in Majorana states originates from Kitaev [2]. The generation of Majorana bound states at surfaces of strong topological insulators (TI) due to the proximity of an *s*-wave superconductor (S) has been explored by Fu and Kane [3, 4] and Sau *et al* [5]. A platform for the generation of Majorana zero modes is a heterostructure consisting of a semiconducting thin film sandwiched between an *s*-wave superconductor and a magnetic insulator [6, 7]. A Majorana state also arises as a zero-energy bound state at the core of a vortex as a consequence of the strong spin–orbit coupling in the TI [1, 3, 5]. For a review see reference [8].

Following Fu and Kane [3, 4] numerous authors investigated the surface states of a 3D TI with proximity induced *s*-wave superconductivity in different geometries [5, 9–11]. Depending on the transparency of the TI/S junction the induced superconducting gap is reduced compared to the parent S gap. The induced gap is energy dependent, but is only a weak function of energy for low-lying excitations, so that we can consider Δ a constant. In the dirty limit the proximity effect has been studied using the Eilenberger/Usadel formalism [12–14] and the Majorana state with the Bogoliubov–de Gennes (BdG) method for a supersymmetric σ model [15].

The electronic structure of a vortex in a 2D topological superconductor has been investigated by numerous authors

* Author to whom any correspondence should be addressed.

[5, 10, 11, 15–19] by solving the BdG equations. The strong spin–orbit coupling leads to spin–momentum locking and a zero-energy Majorana bound state, as a consequence of the Berry phase. The low-energy excitations are equally spaced by the amount of Δ_∞^2/E_F. Vortex bound states in a proximity-induced topological superconductor on a spherical surface have been studied in references [20, 21]. In this geometry the boundary of the topological states is closed corresponding to a vortex anti-vortex pair. Following the proposal by Fu and Kane [3] in reference [5] the excitation gap in a line junction and a trijunction pair linked by a line junction was considered. Durst [22] obtained the scattering cross section for quasi-particles with excitation energy greater that Δ_∞ off the vortex states. A possible application of non-abelian topological order in *s*-wave superfluids of ultracold fermionic atoms has been proposed by Sato *et al* [23].

It is interesting to notice that the problem is closely related to vortex states in superconducting graphene [24]. The two sublattices of the honeycomb structure are parametrized by a pseudospin, which plays the role of the spin in the TI. The BdG equations in superconducting graphene for energies close to the Dirac points (considering the spin, pseudospin and particle–holes) reduce to eight equations which decouple into two equivalent subsets of four equations each. Each subset is then equivalent to the present problem with Dirac interaction [25].

In this paper we study the electronic structure of vortices in superconducting surface states with strong spin–orbit coupling. Most of the above mentioned calculations for the vortex bound states are numerical evaluations of the energy eigenvalues. The purpose of this paper is to present analytical expressions for the low-energy bound state eigenvalues and the eigenfunctions close to the core of an isolated vortex. We solve the BdG equations using the method employed by Caroli, de Gennes and Matricon (CdeGM) [26, 27] for a type II *s*-wave superconductor. Here the BdG equations are solved (i) for small distances ρ (compared to the correlation length ξ) from the core of the vortex, where the superconductor order parameter can be neglected since it vanishes at the center of the core, and (ii) for larger distances, still smaller than ξ, but where the order parameter needs to be taken into account. These two solutions are matched at an intermediate radius. If the matching condition is such that it is independent of the distance from the vortex core, then we have a solution for the entire region of the vortex. This condition as well determines the value of the energy of the bound state inside the vortex core. This way we obtain the entire low-energy spectrum of the bound states, as well as the analytic expression of the corresponding wave functions and the local density of states (LDOS).

We consider the metallic surface states of a 3D TI with proximity induced *s*-wave superconductivity. We simplify the model by directly introducing the superconducting order parameter into the 2D electron gas, since the more tedious problem consisting of the TI interacting with S has already been studied [5, 10]. We consider a superconductor with strong spin–orbit coupling locking spin perpendicular to the momentum (Rashba coupling). The model and the analytic solution for the wave functions are presented in section 2 and appendix A. A zero-energy Majorana state is generated, as a consequence of the strong spin–orbit coupling. The first excited bound state above the zero-energy Majorana mode has energy Δ_∞^2/E_F for $E_F \gg \Delta_\infty$. The Majorana state can be made more robust by reducing E_F [5, 11]. In appendix C we present an analytic semiclassical approach showing that for $E_F = 0$ the first excited state has energy of the order of Δ_∞.

In section 3 we obtain the analytical expression for the LDOS of the bound states. We discuss the dependence of the LDOS on the distance from the vortex center, the energy and the temperature. The particle–hole symmetry is broken in the LDOS as a consequence of the spin–orbit coupling. The bound states are partially spin-polarized. This polarization depends on the distance from the center of the vortex. The energy shift of the bound states with a small magnetic field is also obtained.

Experimentally, systems with large superconducting transition temperature are desirable. A Majorana zero mode was detected via spin-selective Andreev reflections in the heterostructure $Bi_2Te_3/NbSe_2$ [31] and with tunneling scanning spectroscopy in monolayers of the high-temperature superconductor $FeTe_{0.55}Se_{0.45}$ [32]. Another model with strong spin–orbit coupling locking the spin parallel to the momentum (Dirac Hamiltonian) is also frequently invoked (see section 4). The two models can be transformed into each other via a unitary transformation, which is explicitly shown in section 4. Conclusions follow in section 5.

2. Perpendicular spin and momentum locking: Rashba interaction

2.1. Model

We consider the 2D Hamiltonian with spin–orbit coupling given by the Rashba interaction and *s*-wave superconductivity induced via proximity [13, 14]. The electron gas corresponds to the surface states of a TI. The strong spin–orbit interaction couples the spin perpendicular to the momentum. We consider an isolated vortex, assuming a field perpendicular to the plane with $H \ll H_{c2}$ and slightly larger than H_{c1}.

The wave function is a four-component spinor, $\Psi(\mathbf{r}) = [\psi_\uparrow(\mathbf{r})\ \psi_\downarrow(\mathbf{r})\ \psi_\uparrow^\dagger(\mathbf{r})\ \psi_\downarrow^\dagger(\mathbf{r})]^T$, and the Hamiltonian is $\mathcal{H} = \frac{1}{2}\int d^2r \Psi^\dagger(\mathbf{r})\check{\mathcal{H}}_B^\perp(\mathbf{r})\Psi(\mathbf{r})$, where

$$\check{\mathcal{H}}_B^\perp(\mathbf{r}) = \begin{bmatrix} \hat{h}(\mathbf{r}) & \hat{\Delta}(\mathbf{r}) \\ -\hat{\Delta}^*(\mathbf{r}) & -\hat{h}^*(\mathbf{r}) \end{bmatrix} \tag{1}$$

and

$$\hat{h}(\mathbf{r}) = v_F\hat{\boldsymbol{\sigma}}\cdot\left[\left(\mathbf{p} - \frac{e}{c}\mathbf{A}\right)\times\mathbf{e}_z\right] - E_F\ , \tag{2}$$

$$\hat{\Delta}(\mathbf{r}) = \Delta(\mathbf{r})\,i\hat{\sigma}_y\ , \tag{3}$$

where $\mathbf{e}_z$ is the normal vector to the plane.

Here we adopt polar coordinates, (ρ, θ), and write $\Delta(\mathbf{r}) = \Delta(\rho)e^{-i\theta}$, i.e. only one flux quantum is contained in the vortex. $\Delta(\rho)$ is real, vanishes for $\rho = 0$, increases linearly with ρ and saturates at the value Δ_∞ for ρ larger than the

coherence length ξ [28]. Using the same arguments as in references [26, 27] the vector potential and the magnetic field can be neglected for $\rho < \xi$ in equation (2). In polar coordinates $\hat{h}(\mathbf{r})$ can be written as

$$\hat{h}(\rho,\theta) = \begin{bmatrix} -E_{\mathrm{F}} & -\mathrm{i}v_{\mathrm{F}}\,\mathrm{e}^{-\mathrm{i}\theta}\left(\mathrm{i}\dfrac{\partial}{\partial\rho}+\dfrac{1}{\rho}\dfrac{\partial}{\partial\theta}\right) \\ \mathrm{i}v_{\mathrm{F}}\,\mathrm{e}^{\mathrm{i}\theta}\left(\mathrm{i}\dfrac{\partial}{\partial\rho}-\dfrac{1}{\rho}\dfrac{\partial}{\partial\theta}\right) & -E_{\mathrm{F}} \end{bmatrix}, \tag{4}$$

and the field operators expanded as $\Psi(\rho,\theta) = (2\pi)^{-1/2}\sum_\mu \Psi_\mu(\rho)\mathrm{e}^{\mathrm{i}\mu\theta}$, where μ is an integer to have a single-valued wave function. The θ-phase of $\Delta(\mathbf{r})$ can be eliminated via a gauge transformation, yielding a θ dependence of the components of the spinor Ψ_μ of

$$f_j^\mu \;\exp[-\mathrm{i}\theta\hat{\tau}_z(1+\hat{\sigma}_z)/2+\mathrm{i}\mu\theta], \quad j=1,\ldots,4, \tag{5}$$

where f_j^μ is the amplitude of the component j. Applying the spinor to $\hat{h}(\rho,\theta)$ we obtain

$$\hat{h}_\mu(\rho) = \begin{bmatrix} -E_{\mathrm{F}} & v_{\mathrm{F}}\left(\dfrac{\partial}{\partial\rho}+\dfrac{\mu}{\rho}\right) \\ -v_{\mathrm{F}}\left(\dfrac{\partial}{\partial\rho}-\dfrac{\mu-1}{\rho}\right) & -E_{\mathrm{F}} \end{bmatrix}. \tag{6}$$

The first order differential equations satisfied by f_j^μ are

$$v_{\mathrm{F}}\left(\frac{\partial}{\partial\rho}-\frac{\mu-1}{\rho}\right)f_1^\mu(\rho)+\Delta(\rho)f_3^\mu(\rho)+(E+E_{\mathrm{F}})f_2^\mu(\rho)=0, \tag{7}$$

$$v_{\mathrm{F}}\left(\frac{\partial}{\partial\rho}+\frac{\mu}{\rho}\right)f_2^\mu(\rho)+\Delta(\rho)f_4^\mu(\rho)-(E+E_{\mathrm{F}})f_1^\mu(\rho)=0, \tag{8}$$

$$v_{\mathrm{F}}\left(\frac{\partial}{\partial\rho}+\frac{\mu+1}{\rho}\right)f_3^\mu(\rho)+\Delta(\rho)f_1^\mu(\rho)-(E-E_{\mathrm{F}})f_4^\mu(\rho)=0, \tag{9}$$

$$v_{\mathrm{F}}\left(\frac{\partial}{\partial\rho}-\frac{\mu}{\rho}\right)f_4^\mu(\rho)+\Delta(\rho)f_2^\mu(\rho)+(E-E_{\mathrm{F}})f_3^\mu(\rho)=0. \tag{10}$$

These equations are similar to those in reference [10], where the Dirac Hamiltonian (rather than the Rashba interaction) was employed.

2.2. Majorana state

The zero-energy Majorana bound state is obtained from equations (7)–(10) for $E=\mu=0$. We denote $\tilde{\rho}=k_{\mathrm{F}}\rho$. The structure of the equations leads to the solution [10]

$$\begin{aligned} f_1^{\mathrm{M}}(\mathbf{r}) &= CJ_1(\tilde{\rho})\mathrm{e}^{-K(\tilde{\rho})}\;\mathrm{e}^{-\mathrm{i}\theta}, \\ f_2^{\mathrm{M}}(\mathbf{r}) &= -CJ_0(\tilde{\rho})\mathrm{e}^{-K(\tilde{\rho})}, \\ f_3^{\mathrm{M}}(\mathbf{r}) &= CJ_1(\tilde{\rho})\mathrm{e}^{-K(\tilde{\rho})}\;\mathrm{e}^{\mathrm{i}\theta}, \\ f_4^{\mathrm{M}}(\mathbf{r}) &= -CJ_0(\tilde{\rho})\mathrm{e}^{-K(\tilde{\rho})}, \end{aligned} \tag{11}$$

where C is a normalization constant and $K(\tilde{\rho}) = \int_0^{\tilde{\rho}}\mathrm{d}x\Delta(x)/E_{\mathrm{F}}$. The corresponding wave function is

$$\begin{aligned} \hat{\Psi}_{\mathrm{M}} = C\int \mathrm{d}^2r\;\mathrm{e}^{-K(\tilde{\rho})}\Big[&J_1(\tilde{\rho})\mathrm{e}^{-\mathrm{i}\theta}\psi_\uparrow(\mathbf{r})-J_0(\tilde{\rho})\psi_\downarrow(\mathbf{r}) \\ &+J_1(\tilde{\rho})\mathrm{e}^{\mathrm{i}\theta}\psi_\uparrow^\dagger(\mathbf{r})-J_0(\tilde{\rho})\psi_\downarrow^\dagger(\mathbf{r})\Big]\;. \end{aligned} \tag{12}$$

It is easily verified that $\hat{\Psi}_{\mathrm{M}} = \hat{\Psi}_{\mathrm{M}}^\dagger$ and hence the state is a Majorana fermion. The counterpart to this Majorana fermion is placed in the plane far away from the axis of the vortex (large ρ) and hence not a solution of this problem [17].

2.3. Energies and wave functions

The solution for the general case is presented in appendix A. For the energy of the bound states we obtain

$$E_\mu = \mu\int_0^\infty \mathrm{d}x\;\mathrm{e}^{-2K(x)}\frac{\Delta(x)}{x}\Big/\int_0^\infty \mathrm{d}x\;\mathrm{e}^{-2K(x)}. \tag{13}$$

Since the main contribution to the integrals is for $\rho \ll \xi$, where $\Delta(x)$ is linear in x, we arrive at $E_\mu \approx \mu\Delta'/k_{\mathrm{F}}$, where $\Delta' = \mathrm{d}\Delta/\mathrm{d}\rho \approx \Delta_\infty/\xi \approx k_{\mathrm{F}}\Delta_\infty^2/E_{\mathrm{F}}$ and hence

$$E_\mu \approx \mu\frac{\Delta_\infty^2}{E_{\mathrm{F}}}. \tag{14}$$

Approximate expressions for the amplitudes of the wave functions are given by

$$\begin{aligned} f_1^\mu(\mathbf{r}) &= C'J_{\mu-1}(\tilde{\rho})\mathrm{e}^{-K(\tilde{\rho})}\;\mathrm{e}^{\mathrm{i}(\mu-1)\theta}, \\ f_2^\mu(\mathbf{r}) &= C'J_\mu(\tilde{\rho})\mathrm{e}^{-K(\tilde{\rho})}\;\mathrm{e}^{\mathrm{i}\mu\theta}, \\ f_3^\mu(\mathbf{r}) &= -C'J_{\mu+1}(\tilde{\rho})\mathrm{e}^{-K(\tilde{\rho})}\;\mathrm{e}^{\mathrm{i}(\mu+1)\theta}, \\ f_4^\mu(\mathbf{r}) &= C'J_\mu(\tilde{\rho})\mathrm{e}^{-K(\tilde{\rho})}\;\mathrm{e}^{\mathrm{i}\mu\theta}, \end{aligned} \tag{15}$$

and the energy wave function with energy $E=E_\mu$ is then

$$\begin{aligned} \hat{\psi}_E = C'\int \mathrm{d}^2r\;\mathrm{e}^{-K(\tilde{\rho})}\Big[&J_{\mu-1}(\tilde{\rho})\mathrm{e}^{-\mathrm{i}\theta}\psi_\uparrow(\mathbf{r})+J_\mu(\tilde{\rho})\psi_\downarrow(\mathbf{r}) \\ &-J_{\mu+1}(\tilde{\rho})\mathrm{e}^{\mathrm{i}\theta}\psi_\uparrow^\dagger(\mathbf{r})+J_\mu(\tilde{\rho})\psi_\downarrow^\dagger(\mathbf{r})\Big]\mathrm{e}^{\mathrm{i}\mu\theta}\;. \end{aligned} \tag{16}$$

For $\mu \neq 0$ the wave function corresponds to a fermion operator with $E_\mu \neq 0$, while for $\mu = 0$ we have the Majorana state wave function consistent with equation (12) up to an overall minus sign (by noticing that $J_{-1}(\tilde{\rho}) = -J_1(\tilde{\rho})$), which can be absorbed into the normalization constant C'.

3. Local density of states of the bound states

Given the wave functions and energy eigenvalues the one particle Green's function for spin component σ is[29]

$$G_\omega^\sigma(\mathbf{r},\mathbf{r}') = \sum_\mu\left(\frac{u_\mu^\sigma(\mathbf{r})\,u_\mu^{\sigma^*}(\mathbf{r}')}{\omega+\mathrm{i}0-E_\mu}+\frac{v_\mu^\sigma(\mathbf{r})\,v_\mu^{\sigma^*}(\mathbf{r}')}{\omega+\mathrm{i}0+E_\mu}\right), \tag{17}$$

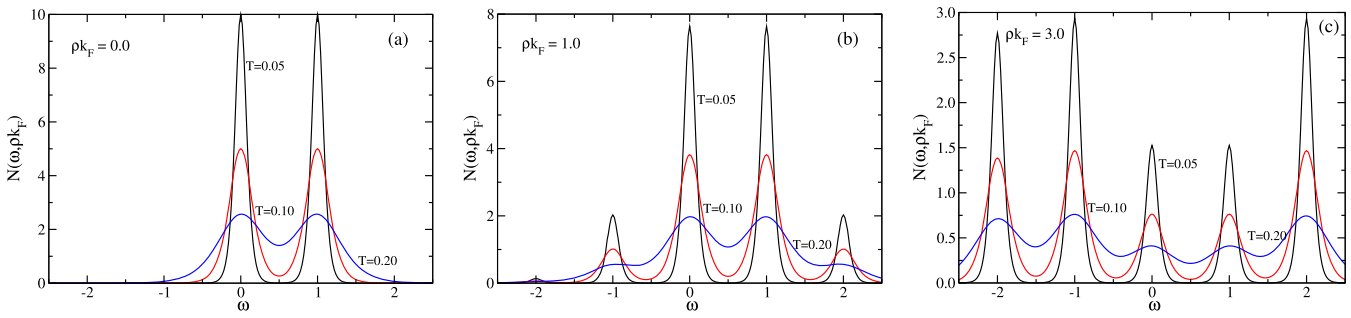

Figure 1. LDOS of the bound states in the vortex as a function of energy ω for three positions from the center of the core: (a) at the center ($\tilde{\rho} = 0.0$), (b) at $\tilde{\rho} = 1.0$ and (c) $\tilde{\rho} = 3.0$. The three curves in each panel represent different temperatures: $T = 0.05$ (black), $T = 0.1$ (red) and $T = 0.2$ (blue). Note that the height of the peaks decreases dramatically with T. In the limit $T \to 0$ the peaks are delta-functions. We chose $K = 0.01\tilde{\rho}^2$. All energies are in units of $\Delta_\infty^2/E_\mathrm{F}$ and the LDOS is in arbitrary units but the same for all three panels. Note that the LDOS is not particle–hole symmetric.

where u and v are the wave functions for particles and holes, i.e. correspond to the functions $f_j^\mu(\mathbf{r})$. The LDOS is given by the imaginary part of the Green's function for $\mathbf{r}' \to \mathbf{r}$

$$N(\omega, \rho) = \sum_{\mu\sigma} \left(|u_\mu^\sigma(\rho)|^2 \delta(\omega - E_\mu) + |v_\mu^\sigma(\rho)|^2 \delta(\omega + E_\mu) \right). \tag{18}$$

For finite temperature the δ function is to be replaced by minus the derivative of the Fermi function [16]. Hence, with increasing temperature the peaks broaden. Similar expressions (without the sum over σ) for the LDOS for each spin projection can be obtained from equation (17).

For our model with Rashba interaction the LDOS is then proportional to (up to a normalization constant for the spinor)

$$N(\omega, \tilde{\rho}) \propto \sum_\mu \left[\left(J_{\mu-1}(\tilde{\rho})^2 + J_\mu(\tilde{\rho})^2 \right) \delta(\omega - E_\mu) + \left(J_{\mu+1}(\tilde{\rho})^2 + J_\mu(\tilde{\rho})^2 \right) \delta(\omega + E_\mu) \right] \mathrm{e}^{-2K(\tilde{\rho})}. \tag{19}$$

This quantity is measurable via scanning tunneling microscopy (STM) by fine-tuning the energy ω at a distance ρ from the core of the vortex. The zero energy Majorana state corresponds to $\mu = 0$ and $E_0 = 0$. Equation (19) is invariant under the transformation $\mu \to -\mu$ (i.e. $E_\mu \to -E_\mu$) and the simultaneous interchange of the particle and hole amplitudes, $u \leftrightarrow v$. However, it is interesting to notice that the LDOS is not particle–hole symmetric.

The latter can be understood with the aid of equation (6). For down-spin the effective angular momentum of the electron is μ, while for up-spin electrons it is $(\mu - 1)$. On the other hand, for down-spin holes it is still μ, but for up-spin holes it is $(\mu + 1)$. Hence, there is a difference between electrons and holes with up-spin and consequently the particle–hole symmetry is broken. The origin of this asymmetry is the Rashba spin–orbit interaction. Hence, the LDOS must be asymmetric as a function of ω.

The LDOS as a function of energy is shown in figure 1 for three distances from the center of the vortex. As a function of ρ the LDOS falls off exponentially due to $K(\tilde{\rho})$. The LDOS also decreases rapidly as a function of temperature. The Majorana state ($\mu = 0$) has always the same intensity as the $\mu = 1$ peak. In general, the LDOS is symmetric about $\omega = 0.5$. At the center of the vortex core ($\tilde{\rho} = 0$) there are only two peaks, namely $\mu = 0$ and 1, as a consequence of the Bessel functions, $J_n(\tilde{\rho})$, which are zero as $\tilde{\rho} \to 0$ for $n \neq 0$. More peaks appear at finite $\tilde{\rho}$. For larger $\tilde{\rho}$ the intensity does not necessarily decrease monotonically with μ as a consequence of the oscillations of the Bessel functions. For instance in figure 1(c) ($\tilde{\rho} = 3$) the $\mu = 2$ peak has higher intensity than the $\mu = 1$ state. This can be understood with the plot of the intensities as a function of $\tilde{\rho}$ presented in figure 2. For $k_\mathrm{F}\rho = 3$ the Majorana peak (and the $\mu = 1$ peak) has a smaller intensity than the $\mu = 2$ and 3 peaks. But for larger energies the intensity of the peaks decreases rapidly. The main maxima of the LDOS form concentric circles about the center of the core with their radius increasing with μ.

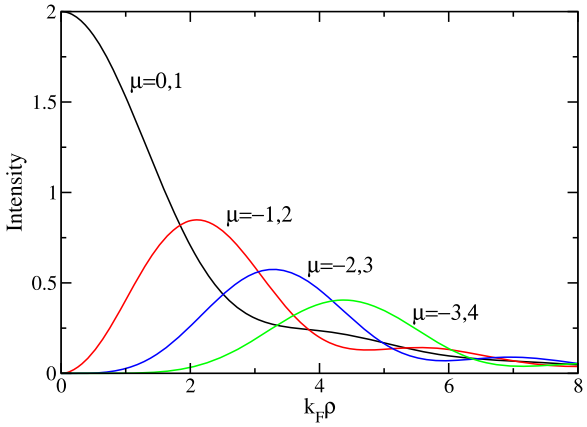

Figure 2. Intensities of the peaks as a function of $k_\mathrm{F}\rho$ for several μ. In general the intensity decreases with $\tilde{\rho}$ and μ, but not necessarily monotonically.

Interesting is also the spin-polarization of the peaks in the LDOS. This is simple at the center of the vortex, $\tilde{\rho} = 0$, where the $\mu = 0$ line (Majorana zero mode) has down-spin and the $\mu = 1$ peak up-spin polarization. For larger $\tilde{\rho}$ the peaks have finite intensity for both spin components, see e.g. figure 3 for $\tilde{\rho} = 1$. The polarization of the peaks should be of interest for spin-selective spectroscopic measurements. Note that the down-spin LDOS is particle–hole symmetric.

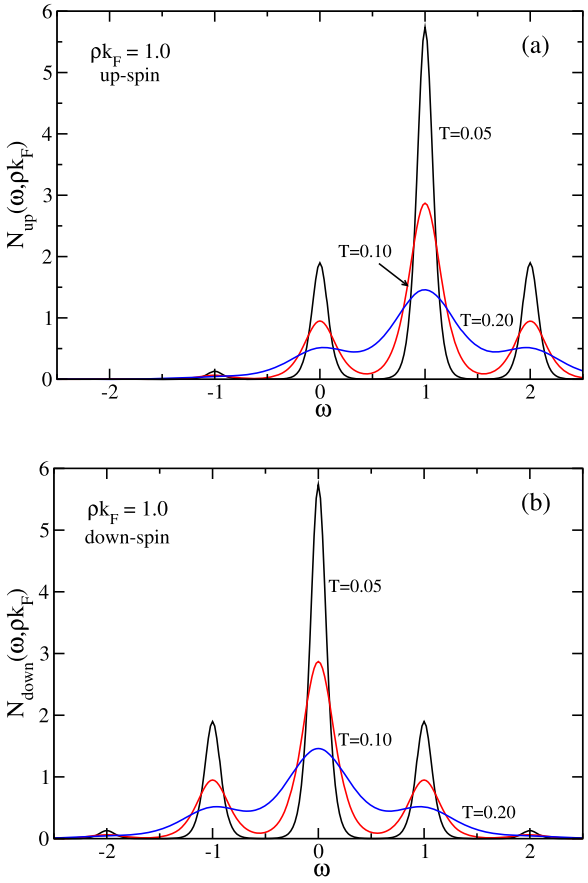

Figure 3. Spin-polarized LDOS (arbitrary units) of the bound states in the vortex as a function of energy ω for $\tilde{\rho} = 1.0$ from the center of the core, (a) up-spin and (b) down-spin polarization. The polarization is consequence of the spin–orbit interaction. The three curves in each panel represent the temperatures $T = 0.05$ (black), $T = 0.1$ (red) and $T = 0.2$ (blue). The sum of the up-spin and down-spin LDOS yield the total LDOS shown figure 1(b). Again, $K = 0.01\tilde{\rho}^2$ and all energies are in units of $\Delta_\infty^2/E_\mathrm{F}$.

The effect of the Zeeman Hamiltonian,

$$H_\mathrm{Z} = \mu_\mathrm{B} H \begin{bmatrix} \sigma_z & 0 \\ 0 & -\sigma_z \end{bmatrix}, \tag{20}$$

on the bound state energy levels can be determined perturbatively using the bound state wave functions, equation (15). To first order the result is,

$$\Delta E_\mu^\mathrm{Z} = \frac{\mu_\mathrm{B} H \int_0^\infty \mathrm{d}\tilde{\rho}\tilde{\rho}\ \mathrm{e}^{-2K(\tilde{\rho})} \left(J_{\mu-1}^2(\tilde{\rho}) - J_{\mu+1}^2(\tilde{\rho})\right)}{\int_0^\infty \mathrm{d}\tilde{\rho}\tilde{\rho}\ \mathrm{e}^{-2K(\tilde{\rho})} \left(J_{\mu-1}^2(\tilde{\rho}) + 2J_\mu^2(\tilde{\rho}) + J_{\mu+1}^2(\tilde{\rho})\right)}. \tag{21}$$

Using $\Delta(\tilde{\rho}) \simeq (\Delta_\infty^2/E_\mathrm{F})\tilde{\rho}$ we have $K(\tilde{\rho}) = (\Delta_\infty^2/E_\mathrm{F}^2)\tilde{\rho}^2/2$. In this case the integrals in (21) can be carried out analytically and, in the limit $\Delta_\infty/E_\mathrm{F} \ll 1$, we find

$$\Delta E_\mu \simeq \mu \frac{\Delta_\infty^2}{E_\mathrm{F}^2} \mu_\mathrm{B} H. \tag{22}$$

Note that the energy of the $\mu = 0$ MZM is unchanged, reflecting its topological protection. For $\mu \neq 0$, we find the magnitude of the energy shifts increase with increasing μ, but since $\mu_\mathrm{B} H \ll \mu_\mathrm{B} H_{c2} \ll E_\mathrm{F}$ these shifts are very small when compared to the bound state energies $E_\mu \simeq \mu\Delta_\infty^2/E_\mathrm{F}$. The gaps are thus not significantly altered.

Similarly, the effect on the bound state energies of the coupling of the field to the orbital degrees of freedom, described by the vector potential contribution to the Hamiltonian which has so far been neglected,

$$H_\mathrm{O} = \begin{bmatrix} -v_\mathrm{F}\vec{\sigma}\cdot\left(\frac{e}{c}\vec{A}\times\hat{e}_z\right) & 0 \\ 0 & v_\mathrm{F}\vec{\sigma}\cdot\left(\frac{e}{c}\vec{A}\times\hat{e}_z\right) \end{bmatrix}, \tag{23}$$

can be taken into account perturbatively. Taking $\vec{A}(\rho) = \frac{1}{2}\rho H\hat{e}_\theta$, the first-order energy shifts we find are,

$$\Delta E_\mu^\mathrm{O} = -\frac{2\mu\frac{eH}{mc}\int_0^\infty \mathrm{d}\tilde{\rho}\tilde{\rho}\ \mathrm{e}^{-2K(\tilde{\rho})} J_\mu^2(\tilde{\rho})}{\int_0^\infty d\tilde{\rho}\tilde{\rho}\ \mathrm{e}^{-2K(\tilde{\rho})} \left(J_{\mu-1}^2(\tilde{\rho}) + 2J_\mu^2(\tilde{\rho}) + J_{\mu+1}^2(\tilde{\rho})\right)}. \tag{24}$$

Taking $K(\tilde{\rho}) = (\Delta_\infty^2/E_\mathrm{F}^2)\tilde{\rho}^2/2$ as above, the integrals in equation (24) can again be carried out analytically. In the limit $\Delta_\infty/E_\mathrm{F} \ll 1$ we find,

$$\Delta E_\mu^\mathrm{O} \simeq -\mu\frac{eH}{2mc}. \tag{25}$$

Again, the topologically protected MZM is unaffected and the magnitude of the energy shifts are seen to grow with μ. These energy shifts can safely be neglected provided $eH/(mc) \ll \Delta_\infty/E_\mathrm{F}^2$ which should hold for the relevant case of $H \ll H_{c2}$.

Experimentally, heterostructures of $Bi_2Te_3/NbSe_2$ (references [30, 31]) and monolayers of the high-temperature superconductor $FeTe_{0.55}Se_{0.45}$ on $SrTiO_3(001)$ (references [32–34]) were investigated. Both systems have the advantage of relatively large superconducting transition temperatures. Note that for both systems only one peak is observed, which is an indication that the first excitation energy is of the order of Δ. In a particularly careful study on $Bi_2Te_3/NbSe_2$ a Majorana zero mode was detected in a vortex with spin-selective Andreev reflection [31]. The zero-bias peak of the tunneling differential conductance at the vortex center is substantially higher when the tip polarization and the external magnetic field are parallel rather than antiparallel to each other, providing direct evidence of a Majorana zero mode.

For the iron-based superconductor, using scanning tunneling spectroscopy, a sharp zero-bias peak was observed inside the vortex core that does not split when moving away from the vortex center [32]. The evolution of the peak under varying magnetic field, temperature, and tunneling barrier is consistent with a nearly pure Majorana bound state. In reference [33] two distinct classes of vortices were found, differing by a half-integer level shift in the energy spectra of the vortex bound states. The level shift is directly tied to the presence (absence) of a zero-bias conductance peak. More recently zero-energy bound states simultaneously appearing at both ends of a 1D atomic line defect were discovered [34].

4. Relation to the Dirac Hamiltonian

4.1. Model

Another popular system to study bound states in a vortex is the 2D Dirac model with s-wave superconductivity induced via proximity [3, 10, 16]. The electron gas corresponds to the surface states of a TI. The strong spin–orbit interaction couples the spin parallel to the momentum. As before we consider an isolated vortex, assuming the field perpendicular to the plane. The four-component spinor Ψ and the Hamiltonian $\mathcal{H}$ are defined as in section 2 but with

$$\check{\mathcal{H}}_B^{\parallel}(\mathbf{r}) = \begin{bmatrix} \hat{h}(\mathbf{r}) & \hat{\Delta}(\mathbf{r}) \\ -\hat{\Delta}^*(\mathbf{r}) & -\hat{h}^*(\mathbf{r}) \end{bmatrix} \tag{26}$$

and

$$\hat{h}(\mathbf{r}) = v_{\mathrm{F}}\hat{\boldsymbol{\sigma}}\cdot\left(\mathbf{p} - \frac{e}{c}\mathbf{A}\right) - E_{\mathrm{F}}. \tag{27}$$

In polar coordinates $\Delta(\mathbf{r}) = \Delta(\rho)\mathrm{e}^{-\mathrm{i}\theta}$ and

$$\hat{h}(\rho,\theta) = \begin{bmatrix} -E_{\mathrm{F}} & -\mathrm{i}v_{\mathrm{F}}\,\mathrm{e}^{-\mathrm{i}\theta}\left(\dfrac{\partial}{\partial\rho} - \dfrac{\mathrm{i}\partial}{\rho\partial\theta}\right) \\ -\mathrm{i}v_{\mathrm{F}}\,\mathrm{e}^{\mathrm{i}\theta}\left(\dfrac{\partial}{\partial\rho} + \dfrac{\mathrm{i}\partial}{\rho\partial\theta}\right) & -E_{\mathrm{F}} \end{bmatrix}, \tag{28}$$

As in section 2 we expand the field operators in partial waves $\mathrm{e}^{\mathrm{i}\mu\theta}$, where μ is an integer to have a single-valued wave function. The θ-phase of $\Delta(\mathbf{r})$ can be eliminated via a gauge transformation. The θ dependence of the components of the spinor Ψ_μ are again given by equation (5) and applying the spinor to $\hat{h}(\rho,\theta)$ we have

$$\hat{h}(\rho,\theta) = \begin{bmatrix} -E_{\mathrm{F}} & -\mathrm{i}v_{\mathrm{F}}\,\mathrm{e}^{-\mathrm{i}\theta}\left(\dfrac{\partial}{\partial\rho} + \dfrac{\mu}{\rho}\right) \\ -\mathrm{i}v_{\mathrm{F}}\,\mathrm{e}^{\mathrm{i}\theta}\left(\dfrac{\partial}{\partial\rho} - \dfrac{\mu-1}{\rho}\right) & -E_{\mathrm{F}} \end{bmatrix}. \tag{29}$$

The first order differential equations satisfied by the amplitudes f_j^μ are

$$-\mathrm{i}v_{\mathrm{F}}\left(\frac{\partial}{\partial\rho} - \frac{\mu-1}{\rho}\right) f_1^\mu(\rho) - \Delta(\rho) f_3^\mu(\rho) - (E+E_{\mathrm{F}}) f_2^\mu(\rho) = 0, \tag{30}$$

$$-\mathrm{i}v_{\mathrm{F}}\left(\frac{\partial}{\partial\rho} + \frac{\mu}{\rho}\right) f_2^\mu(\rho) + \Delta(\rho) f_4^\mu(\rho) - (E+E_{\mathrm{F}}) f_1^\mu(\rho) = 0, \tag{31}$$

$$-\mathrm{i}v_{\mathrm{F}}\left(\frac{\partial}{\partial\rho} + \frac{\mu+1}{\rho}\right) f_3^\mu(\rho) + \Delta(\rho) f_1^\mu(\rho) - (E-E_{\mathrm{F}}) f_4^\mu(\rho) = 0, \tag{32}$$

$$-\mathrm{i}v_{\mathrm{F}}\left(\frac{\partial}{\partial\rho} - \frac{\mu}{\rho}\right) f_4^\mu(\rho) - \Delta(\rho) f_2^\mu(\rho) - (E-E_{\mathrm{F}}) f_3^\mu(\rho) = 0. \tag{33}$$

These equations are similar to those in references [10, 16], where slightly different model definitions have been considered.

4.2. Spin rotation transformation

We now present the unitary transformation mapping the Hamiltonian with parallel spin–momentum locking (section 4), $\check{\mathcal{H}}_B^{\parallel}$ (equation (27)), onto the model with Rashba interaction (perpendicular coupling, section 2), $\check{\mathcal{H}}_B^{\perp}$ (equation (2)). Consider the four-dimensional unitary matrix

$$\begin{aligned} U &= \begin{bmatrix} \mathrm{e}^{\mathrm{i}(\pi/4)\sigma_z} & 0 \\ 0 & \mathrm{e}^{-\mathrm{i}(\pi/4)\sigma_z} \end{bmatrix} \\ &= \begin{bmatrix} (1+\mathrm{i}\sigma_z)/\sqrt{2} & 0 \\ 0 & (1-\mathrm{i}\sigma_z)/\sqrt{2} \end{bmatrix}. \end{aligned} \tag{34}$$

It is now straightforward to show that $\check{\mathcal{H}}_B^{\perp} = U\check{\mathcal{H}}_B^{\parallel}U^\dagger$,

$$\begin{aligned} U\check{\mathcal{H}}_B^{\parallel}U^\dagger &= \begin{bmatrix} \mathrm{e}^{\mathrm{i}(\pi/4)\sigma_z} & 0 \\ 0 & \mathrm{e}^{-\mathrm{i}(\pi/4)\sigma_z} \end{bmatrix} \begin{bmatrix} \sigma_x p_x + \sigma_y p_y - E_{\mathrm{F}} & \mathrm{i}\sigma_y\Delta \\ -\mathrm{i}\sigma_y\Delta^* & -(\sigma_x p_x + \sigma_y p_y)^* + E_{\mathrm{F}} \end{bmatrix} \begin{bmatrix} \mathrm{e}^{-\mathrm{i}(\pi/4)\sigma_z} & 0 \\ 0 & \mathrm{e}^{\mathrm{i}(\pi/4)\sigma_z} \end{bmatrix} \\ &= \begin{bmatrix} (-\sigma_y p_x + \sigma_x p_y) - E_{\mathrm{F}} & \mathrm{i}\sigma_y\Delta \\ -\mathrm{i}\sigma_y\Delta^* & -(-\sigma_y p_x + \sigma_x p_y)^* + E_{\mathrm{F}} \end{bmatrix} = \check{\mathcal{H}}_B^{\perp}. \end{aligned} \tag{35}$$

The wave functions, including the phase factors B_j, for the two types of spin–momentum lockings also transform according to U.

5. Conclusions

We studied the bound states in the core of a vortex of a two-dimensional topological superconductor with Rashba interaction by solving the BdG equations following the procedure outlined by CdeGM [26]. The electron gas corresponds to the surface states of a TI with the superconductivity induced via proximity effect from a nearby s wave superconductor [3, 5, 9, 10]. The momentum and the spin are locked perpendicularly due to the strong spin–orbit interaction. However, the results for the bound states in the core of the vortex are independent of the kind of spin–orbit coupling (as long as it is strong), e.g. parallel or perpendicular spin–momentum locking. In subsection 4.2 we present the unitary transformation connecting the

Hamiltonians for parallel and perpendicular spin and momentum locking (spin-rotation). The characteristic energy scale for the spacing of the energy levels is Δ_∞^2/E_F.

The calculation yields a string of fermion bound states with energy E_μ, $\mu \neq 0$ and a bound state with Majorana statistics for $\mu = 0$ and $E = 0$. While in previous studies the results are mainly numerical, we obtained analytical expressions for the energy spectrum and the wave functions. The wave functions consist of products of a Bessel function and an exponential decay as function of the distance to the core of the vortex. The characteristic function determining the fall off is $\exp[-\int_0^\rho \mathrm{d}\rho'\Delta(\rho')/v_F]$. Given the wave functions we obtained an analytic expression of the LDOS for the bound states. This quantity is, in principle, experimentally accessible via STM [32]. The maximum LDOS of the Majorana state is at $\rho = 0$, while for larger μ the maxima as function of ρ form concentric circles with a radius that increases with μ.

The main difference between the ordinary superconductor and the topological superconducting gas is the spin-locking. In the latter in a closed path the spin is forced to follow the momentum giving rise to a non-trivial Berry phase of 1/2. This converts the half-integer quantum numbers into integer ones and opens the possibility to the existence of a Majorana fermion.

We studied the LDOS as a function of external frequency, temperature and distance from the center of the vortex. The peaks in the LDOS decrease rapidly with temperature due to the smearing of the Fermi function. Outside the vortex-core, the height of the peaks also decreases fast with the distance from the vortex core. It is interesting to notice that the particle–hole symmetry is broken in the LDOS as a consequence of the spin–orbit coupling. This can be traced to equation (6). The bound states are partially spin-polarized. For instance, the Majorana peak is a pure down-spin state at the core of the vortex ($\tilde{\rho} = 0$), but becomes partially polarized away from the center. The polarization of all states depends on the distance from the vortex core.

The energy shift of the bound states in a small magnetic field (Zeeman and orbital contributions) has also been obtained. The topologically protected MZM is unaffected by the magnetic field. The magnitude of the energy shifts grows with μ, but is small compared to Δ_∞^2/E_F, so that the gaps are not significantly altered. This is consistent with our initial assumption in section 2.1.

The experimental search for Majorana zero modes was successful in two systems, namely, heterostructures of $Bi_2Te_3/NbSe_2$ [30, 31] and monolayers of the high-temperature superconductor $FeTe_{0.55}Se_{0.45}$ on $SrTiO_3(001)$ [32, 33]. Both systems have the advantage of relatively large superconducting transition temperatures.

Within the range of validity of the present calculation ($|E| \ll \Delta_\infty \ll E_F$), the gap between the Majorana state and the first excited fermion state is rather small, even for high-T_c superconductors. Hence, very low temperatures are required, unless E_F is reduced to close to the apex of the Dirac Hamiltonian. Although this is beyond the validity of our results, we do not expect qualitative changes in the results. Indeed it has been numerically shown in references [5, 11] that the first excited state above the Majorana bound state can have an excitation energy of the order of Δ_∞. This would be a necessary condition for the use of this Majorana state in quantum computing.

In appendix C we present a semiclassical approach for the excited states. For $E_F \gg \Delta_\infty$ we reproduce the results above, while for $E_F \approx 0$ we obtain the first excited state at $\sqrt{2}\Delta_\infty$. This value is about 50% larger than previous numerical calculations in reference [5, 11]. Our result is expected to be an overestimate since quantum fluctuations are neglected. The electronic spectrum of the vortex is then sufficiently robust for applications in quantum computing.

An alternative way to enhance the gap between the Majorana zero mode and the first excitation and thus to stabilize the Majorana state is to introduce a cylindrical hole in the superconductor [10, 11]. A similar approach using a heterostructure consisting of a magnetic insulator, a TI and a superconductor was proposed by Sau *et al* [6]. The carved hole serves as a pinning center for a vortex. Inside the hole the superconductor order parameter is zero. The number of trapped flux quanta is fine-tuned by the magnetic field perpendicular to the plane. Only for an odd number of trapped flux quanta is there a Majorana zero-mode. If the superconductor consists of an island a second Majorana fermion emerges at the edge of the island. In the case of our models the conjugated Majorana state lies in the plane far away from the core of the vortex.

Acknowledgments

The authors thank Prof. P Xiong for helpful comments. The support by the U.S. Defense Advanced Research Projects Agency (DARPA) under Agreement No. D18AC00010 is acknowledged. The National High Magnetic Field Laboratory is supported by National Science Foundation Cooperative Agreement No. DMR1644779 and the State of Florida.

Appendix A. Solution of the Bogoliubov–de Gennes equations

Using the method by CdeGM [26, 27] the equations are solved (i) for small distances ρ, and (ii) for larger distances (but smaller than ξ). These two solutions are then matched at an intermediate radius, ρ_c. If the matching condition is such that it is independent of the distance from the vortex core, the solution is valid for the entire region of the vortex. This condition as well determines the values of the energies of the bound states inside the vortex core.

A.1. Solution for $\rho < \rho_c$

It is convenient to convert the first order differential equations, (7)–(10), into second order ones. From equation (7) we can express $f_2^\mu(\rho)$ and insert it into equation (8). Similar substitutions can be done for the remaining equations. Defining $q_p = (E_F + E)/v_F$ and $q_h = (E_F - E)/v_F$ (for particles and holes,

respectively) we obtain

$$\left[\frac{\partial^2}{\partial\rho^2}+\frac{1}{\rho}\frac{\partial}{\partial\rho}-\frac{(\mu-1)^2}{\rho^2}+q_{\rm p}^2\right]f_1^\mu = \frac{q_{\rm p}}{v_{\rm F}}\Delta(\rho)f_4^\mu-\left(\frac{\partial}{\partial\rho}+\frac{\mu}{\rho}\right)\frac{\Delta(\rho)}{v_{\rm F}}f_3^\mu, \tag{36}$$

$$\left[\frac{\partial^2}{\partial\rho^2}+\frac{1}{\rho}\frac{\partial}{\partial\rho}-\frac{\mu^2}{\rho^2}+q_{\rm p}^2\right]f_2^\mu = -\frac{q_{\rm p}}{v_{\rm F}}\Delta(\rho)f_3^\mu-\left(\frac{\partial}{\partial\rho}-\frac{\mu-1}{\rho}\right)\frac{\Delta(\rho)}{v_{\rm F}}f_4^\mu, \tag{37}$$

$$\left[\frac{\partial^2}{\partial\rho^2}+\frac{1}{\rho}\frac{\partial}{\partial\rho}-\frac{(\mu+1)^2}{\rho^2}+q_{\rm h}^2\right]f_3^\mu = \frac{q_{\rm h}}{v_{\rm F}}\Delta(\rho)f_2^\mu-\left(\frac{\partial}{\partial\rho}-\frac{\mu}{\rho}\right)\frac{\Delta(\rho)}{v_{\rm F}}f_1^\mu, \tag{38}$$

$$\left[\frac{\partial^2}{\partial\rho^2}+\frac{1}{\rho}\frac{\partial}{\partial\rho}-\frac{\mu^2}{\rho^2}+q_{\rm h}^2\right]f_4^\mu = -\frac{q_{\rm h}}{v_{\rm F}}\Delta(\rho)f_1^\mu-\left(\frac{\partial}{\partial\rho}+\frac{\mu+1}{\rho}\right)\frac{\Delta(\rho)}{v_{\rm F}}f_2^\mu. \tag{39}$$

Since $\Delta(\rho)$ increases linearly from zero, we may neglect $\Delta(\rho)$ for $\rho<\rho_{\rm c}$. The solutions for $\rho<\rho_{\rm c}$ are then

$$\begin{aligned} f_1^\mu(q_{\rm p}\rho)&=A_1^\mu J_{\mu-1}(q_{\rm p}\rho),\\ f_2^\mu(q_{\rm p}\rho)&=A_2^\mu J_{\mu}(q_{\rm p}\rho),\\ f_3^\mu(q_{\rm h}\rho)&=A_3^\mu J_{\mu+1}(q_{\rm h}\rho),\\ f_4^\mu(q_{\rm h}\rho)&=A_4^\mu J_{\mu}(q_{\rm h}\rho), \end{aligned} \tag{40}$$

where $J_\nu(z)$ are Bessel functions. The constants A_j^μ are not all independent. Substituting the solution (40) into the first order differential equations we have $A_1^\mu=A_2^\mu$ and $A_3^\mu=-A_4^\mu$. The constants A_1 and A_4 are independent for $\Delta=0$, but become coupled when $\Delta\neq0$, namely, $A_1=\sqrt{1+\tilde{E}}$ and $A_4=\sqrt{1-\tilde{E}}$, where $\tilde{E}=E/(v_{\rm F}k_{\rm F})$ (see part A.3 of appendix A).

A.2. Solution for $\rho>\rho_{\rm c}$

Δ plays a relevant role for $\rho>\rho_{\rm c}$. We write the solution as a product of a Hankel function times an envelope function, $f_j(\tilde{\rho})=B_j[H_\mu^{(1)}(\tilde{\rho})g_j(\tilde{\rho})+\text{c.c.}]$, where the B_j are constants. Here we use Bardeen *et al*'s [29] choice for the order of the Hankel function, while CdeGM [26] considered $H_m^{(1)}$ with $m=\sqrt{\mu^2+\frac{1}{4}}$. Both are viable ways to proceed. We postulate $B_1=B_2=-B_3=B_4=\frac{1}{2}B$, where B is the normalization constant equated to one for simplicity. The relative phases of the B_j are the same as in equation (40). The verification that this choice of B_j is the correct one follows in part A.3 of this appendix, where we match the wave function for $\rho<\rho_{\rm c}$ to $\rho>\rho_{\rm c}$. We introduce again the dimensionless variables $\tilde{\rho}=k_{\rm F}\rho$, $\tilde{E}=E/(k_{\rm F}v_{\rm F})$ and $\tilde{\Delta}=\Delta/(k_{\rm F}v_{\rm F})$, and further assume that for $\rho\ll\xi$, $\mathrm{d}\Delta(\tilde{\rho})/\mathrm{d}\tilde{\rho}=\Delta'$, where Δ' is a constant.

Next we insert the ansatz for $f_j(\tilde{\rho})$ into equations (36)–(39), use the differential equation satisfied by the Hankel function and divide the equations by $H_\mu^{(1)}(\tilde{\rho})$. The quantity $[\mathrm{d}H_\mu^{(1)}(\tilde{\rho})/\mathrm{d}\tilde{\rho}]/H_\mu^{(1)}(\tilde{\rho})$ is obtained using the asymptotic expansion of $H_\mu^{(1)}(\tilde{\rho})$ for large argument (see appendix B)

$$\frac{1}{H_\mu^{(1)}(\tilde{\rho})}\frac{\mathrm{d}H_\mu^{(1)}(\tilde{\rho})}{\mathrm{d}\tilde{\rho}}\sim-\frac{1}{2\tilde{\rho}}+\mathrm{i}. \tag{41}$$

Note that the next order in the expansion in equation (41) does not add relevant terms to the order in $1/\tilde{\rho}$ considered here. This way we arrive at the following four coupled second order differential equations for the functions $g_j(\tilde{\rho})$:

$$\frac{\mathrm{d}^2g_1}{\mathrm{d}\tilde{\rho}^2}+2\mathrm{i}\frac{\mathrm{d}g_1}{\mathrm{d}\tilde{\rho}}+\left[\tilde{E}^2+2\tilde{E}+\frac{2\,\mu-1}{\tilde{\rho}^2}\right]g_1 = \tilde{\Delta}(1+\tilde{E})g_4+\tilde{\Delta}\frac{\mathrm{d}g_3}{\mathrm{d}\tilde{\rho}}+\left[\frac{2\,\mu+1}{2\tilde{\rho}}+\mathrm{i}\right]\tilde{\Delta}g_3, \tag{42}$$

$$\frac{\mathrm{d}^2g_2}{\mathrm{d}\tilde{\rho}^2}+2\mathrm{i}\frac{\mathrm{d}g_2}{\mathrm{d}\tilde{\rho}}+\left[\tilde{E}^2+2\tilde{E}\right]g_2 = \tilde{\Delta}(1+\tilde{E})g_3-\tilde{\Delta}\frac{\mathrm{d}g_4}{\mathrm{d}\tilde{\rho}}+\left[\frac{2\,\mu-3}{2\tilde{\rho}}-\mathrm{i}\right]\tilde{\Delta}g_4, \tag{43}$$

$$\frac{\mathrm{d}^2g_3}{\mathrm{d}\tilde{\rho}^2}+2\mathrm{i}\frac{\mathrm{d}g_3}{\mathrm{d}\tilde{\rho}}+\left[\tilde{E}^2-2\tilde{E}-\frac{2\,\mu+1}{\tilde{\rho}^2}\right]g_3 = -\tilde{\Delta}(1-\tilde{E})g_2+\tilde{\Delta}\frac{\mathrm{d}g_1}{\mathrm{d}\tilde{\rho}}-\left[\frac{2\,\mu-1}{2\tilde{\rho}}-\mathrm{i}\right]\tilde{\Delta}g_1, \tag{44}$$

$$\frac{\mathrm{d}^2g_4}{\mathrm{d}\tilde{\rho}^2}+2\mathrm{i}\frac{\mathrm{d}g_4}{\mathrm{d}\tilde{\rho}}+\left[\tilde{E}^2-2\tilde{E}\right]g_4 = -\tilde{\Delta}(1-\tilde{E})g_1-\tilde{\Delta}\frac{\mathrm{d}g_2}{\mathrm{d}\tilde{\rho}}-\left[\frac{2\,\mu+3}{2\tilde{\rho}}+\mathrm{i}\right]\tilde{\Delta}g_2. \tag{45}$$

Equations (42)–(45) are solved perturbatively. To zeroth order we have, keeping the dominant terms,

$$2\mathrm{i}\frac{\mathrm{d}}{\mathrm{d}\tilde{\rho}}\begin{bmatrix}g_1^{(0)}\\g_2^{(0)}\\g_3^{(0)}\\g_4^{(0)}\end{bmatrix}=\tilde{\Delta}\begin{bmatrix}g_4^{(0)}\\g_3^{(0)}\\-g_2^{(0)}\\-g_1^{(0)}\end{bmatrix}+\mathrm{i}\tilde{\Delta}\begin{bmatrix}g_3^{(0)}\\-g_4^{(0)}\\g_1^{(0)}\\-g_2^{(0)}\end{bmatrix}, \tag{46}$$

while the remaining terms in equations (42)–(45) will be treated in first order perturbation, $g_j^{(1)}$. The solution of equation (46) is

$$\begin{aligned} g_1^{(0)}(\tilde{\rho})&=C\,\mathrm{e}^{-K(\tilde{\rho})}, & g_2^{(0)}(\tilde{\rho})&=-\mathrm{i}C\,\mathrm{e}^{-K(\tilde{\rho})},\\ g_3^{(0)}(\tilde{\rho})&=-C\,\mathrm{e}^{-K(\tilde{\rho})}, & g_4^{(0)}(\tilde{\rho})&=-\mathrm{i}C\,\mathrm{e}^{-K(\tilde{\rho})}, \end{aligned} \tag{47}$$

where $K(\tilde{\rho}) = \int_0^{\tilde{\rho}} \mathrm{d}x\tilde{\Delta}(x)$ has been defined before, $C = \mathrm{e}^{\mathrm{i}\gamma}$ and γ is to be determined.

The equations for $g_j^{(1)}$ are

$$
\begin{aligned}
&2\mathrm{i}\frac{\mathrm{d}}{\mathrm{d}\tilde{\rho}}\begin{bmatrix} g_1^{(1)} \\ g_2^{(1)} \\ g_3^{(1)} \\ g_4^{(1)} \end{bmatrix} - \tilde{\Delta}\begin{bmatrix} g_4^{(1)} \\ g_3^{(1)} \\ -g_2^{(1)} \\ -g_1^{(1)} \end{bmatrix} - \mathrm{i}\tilde{\Delta}\begin{bmatrix} g_3^{(1)} \\ -g_4^{(1)} \\ g_1^{(1)} \\ -g_2^{(1)} \end{bmatrix} \\
&\quad = -\frac{\mathrm{d}^2}{\mathrm{d}\tilde{\rho}^2}\begin{bmatrix} g_1^{(0)} \\ g_2^{(0)} \\ g_3^{(0)} \\ g_4^{(0)} \end{bmatrix} - \begin{bmatrix} (\tilde{E}^2 + 2\tilde{E} + \dfrac{2\ \mu - 1}{\tilde{\rho}^2})g_1^{(0)} \\ (\tilde{E}^2 + 2\tilde{E})g_2^{(0)} \\ (\tilde{E}^2 - 2\tilde{E} - \dfrac{2\ \mu + 1}{\tilde{\rho}^2})g_3^{(0)} \\ (\tilde{E}^2 - 2\tilde{E})g_4^{(0)} \end{bmatrix} \\
&\qquad + \tilde{\Delta}\tilde{E}\begin{bmatrix} g_4^{(0)} \\ g_3^{(0)} \\ g_2^{(0)} \\ g_1^{(0)} \end{bmatrix} + \tilde{\Delta}\frac{\mathrm{d}}{\mathrm{d}\tilde{\rho}}\begin{bmatrix} g_3^{(0)} \\ -g_4^{(0)} \\ g_1^{(0)} \\ -g_2^{(0)} \end{bmatrix} + \frac{\tilde{\Delta}}{2\tilde{\rho}}\begin{bmatrix} (2\ \mu + 1)g_3^{(0)} \\ (2\ \mu - 3)g_4^{(0)} \\ -(2\ \mu - 1)g_1^{(0)} \\ -(2\ \mu + 3)g_2^{(0)} \end{bmatrix}.
\end{aligned}
\tag{48}
$$

Inserting our solutions for $g_j^{(0)}$ into equation (48), and with the ansatz $g_1^{(1)} = Ca_1\ \mathrm{e}^{-K}$, $g_2^{(1)} = -\mathrm{i}Ca_2\ \mathrm{e}^{-K}$, $g_3^{(1)} = -Ca_3\ \mathrm{e}^{-K}$ and $g_4^{(1)} = -\mathrm{i}Ca_4\ \mathrm{e}^{-K}$, we obtain

$$
\begin{aligned}
&2\mathrm{i}\frac{\mathrm{d}}{\mathrm{d}\tilde{\rho}}\begin{bmatrix} a_1 \\ -\mathrm{i}a_2 \\ -a_3 \\ -\mathrm{i}a_4 \end{bmatrix} - 2\mathrm{i}\tilde{\Delta}\begin{bmatrix} a_1 \\ -\mathrm{i}a_2 \\ -a_3 \\ -\mathrm{i}a_4 \end{bmatrix} - \tilde{\Delta}\begin{bmatrix} -\mathrm{i}a_4 \\ -a_3 \\ \mathrm{i}a_2 \\ -a_1 \end{bmatrix} - \mathrm{i}\tilde{\Delta}\begin{bmatrix} -a_3 \\ \mathrm{i}a_4 \\ a_1 \\ \mathrm{i}a_2 \end{bmatrix} \\
&\quad = \left(\frac{\tilde{\Delta}}{\tilde{\rho}} - \tilde{\Delta}^2\right)\begin{bmatrix} 1 \\ -\mathrm{i} \\ -1 \\ -\mathrm{i} \end{bmatrix} - \begin{bmatrix} \left(\tilde{E}^2 + 2\tilde{E} + \dfrac{2\ \mu - 1}{\tilde{\rho}^2}\right) \\ -\mathrm{i}(\tilde{E}^2 + 2\tilde{E}) \\ -\left(\tilde{E}^2 - 2\tilde{E} - \dfrac{2\ \mu + 1}{\tilde{\rho}^2}\right) \\ -\mathrm{i}(\tilde{E}^2 - 2\tilde{E}) \end{bmatrix} \\
&\qquad + \tilde{\Delta}\tilde{E}\begin{bmatrix} -\mathrm{i} \\ -1 \\ -\mathrm{i} \\ 1 \end{bmatrix} - \tilde{\Delta}^2\begin{bmatrix} -1 \\ \mathrm{i} \\ 1 \\ \mathrm{i} \end{bmatrix} + \frac{\tilde{\Delta}}{2\tilde{\rho}}\begin{bmatrix} -(2\mu + 1) \\ -\mathrm{i}(2\mu - 3) \\ -(2\mu - 1) \\ \mathrm{i}(2\mu + 3) \end{bmatrix}.
\end{aligned}
\tag{49}
$$

Since all the terms are proportional to $\mathrm{e}^{-K(\tilde{\rho})}$, this factor has been cancelled out. After cancellations of $\tilde{\Delta}^2$-terms, the differential equations for a_j are

$$
\begin{aligned}
&2\frac{\mathrm{d}}{\mathrm{d}\tilde{\rho}}\begin{bmatrix} a_1 \\ -\mathrm{i}a_2 \\ -a_3 \\ -\mathrm{i}a_4 \end{bmatrix} + \tilde{\Delta}\begin{bmatrix} (a_3 + a_4) - 2a_1 \\ (a_3 + a_4) - 2a_2 \\ (a_1 + a_2) - 2a_3 \\ (a_1 + a_2) - 2a_4 \end{bmatrix} \\
&\quad = -\begin{bmatrix} \mathrm{i}\left(\tilde{E}^2 + 2\tilde{E} + \dfrac{2\ \mu - 1}{\tilde{\rho}^2}\right) \\ \mathrm{i}(\tilde{E}^2 + 2\tilde{E}) \\ \mathrm{i}\left(\tilde{E}^2 - 2\tilde{E} - \dfrac{2\ \mu + 1}{\tilde{\rho}^2}\right) \\ \mathrm{i}(\tilde{E}^2 - 2\tilde{E}) \end{bmatrix} + \tilde{\Delta}\tilde{E}\begin{bmatrix} -1 \\ -1 \\ 1 \\ 1 \end{bmatrix} \\
&\qquad + \frac{\tilde{\Delta}}{2\tilde{\rho}}\begin{bmatrix} \mathrm{i}(2\mu - 1) \\ -\mathrm{i}(2\mu - 1) \\ -\mathrm{i}(2\mu + 1) \\ \mathrm{i}(2\mu + 1) \end{bmatrix}.
\end{aligned}
\tag{50}
$$

These equations decouple by taking linear combinations:

$$
\begin{aligned}
&2\frac{\mathrm{d}}{\mathrm{d}\tilde{\rho}}(a_1 - a_2) - 2\tilde{\Delta}(a_1 - a_2) = \mathrm{i}\frac{2\mu - 1}{\tilde{\rho}^2} + \mathrm{i}\frac{\tilde{\Delta}}{\tilde{\rho}}(2\mu - 1), \\
&2\frac{\mathrm{d}}{\mathrm{d}\tilde{\rho}}(a_3 - a_4) - 2\tilde{\Delta}(a_3 - a_4) = -\mathrm{i}\frac{2\mu + 1}{\tilde{\rho}^2} - \mathrm{i}\frac{\tilde{\Delta}}{\tilde{\rho}}(2\mu + 1), \\
&\frac{\mathrm{d}}{\mathrm{d}\tilde{\rho}}(a_1 + a_2 + a_3 + a_4) = 2\mathrm{i}\tilde{E}^2 - \mathrm{i}\frac{1}{\tilde{\rho}^2}, \\
&\frac{\mathrm{d}}{\mathrm{d}\tilde{\rho}}(a_1 + a_2 - a_3 - a_4) - 2\tilde{\Delta}(a_1 + a_2 - a_3 - a_4) \\
&\qquad = 4\mathrm{i}\tilde{E} + \mathrm{i}\frac{2\mu}{\tilde{\rho}^2} - 2\tilde{\Delta}\tilde{E}.
\end{aligned}
\tag{51}
$$

The integration of the decoupled differential equations yields

$$
a_1 - a_2 = -\mathrm{i}(\mu - \frac{1}{2})\int_{\tilde{\rho}}^{\infty} \mathrm{d}x\ \exp[K(\tilde{\rho}) - K(x)]\left[\frac{1}{x^2} + \frac{\tilde{\Delta}(x)}{x}\right], \tag{52}
$$

$$
a_3 - a_4 = \mathrm{i}(\mu + \frac{1}{2})\int_{\tilde{\rho}}^{\infty} \mathrm{d}x\ \exp[K(\tilde{\rho}) - K(x)]\left[\frac{1}{x^2} + \frac{\tilde{\Delta}(x)}{x}\right], \tag{53}
$$

$$
a_1 + a_2 + a_3 + a_4 = 2\mathrm{i}\tilde{E}^2\tilde{\rho} + \frac{\mathrm{i}}{\tilde{\rho}}, \tag{54}
$$

$$
\begin{aligned}
&a_1 + a_2 - a_3 - a_4 \\
&\quad = -\mathrm{i}\int_{\tilde{\rho}}^{\infty} \mathrm{d}x\ \exp[2K(\tilde{\rho}) - 2K(x)]\left[4\tilde{E} + \frac{2\ \mu}{x^2}\right] \\
&\qquad - 2\int_0^{\tilde{\rho}} \mathrm{d}x\ \exp[2K(\tilde{\rho}) - 2K(x)]\tilde{E}\tilde{\Delta}(x).
\end{aligned}
\tag{55}
$$

The first term in equation (54) and the last term in equation (55) are of third order in the small parameters $\tilde{\Delta}(\tilde{\rho})$, $\tilde{E}$ and $\tilde{\rho}$ and can be neglected. The remaining two integrals can be simplified by integrating by parts

$$
\begin{aligned}
&\int_{\tilde{\rho}}^{\infty} \mathrm{d}x\ \exp[2K(\tilde{\rho}) - 2K(x)]\left[\tilde{E} + \frac{\mu}{2x^2}\right] \\
&\quad = -\tilde{E}\tilde{\rho} + \frac{\mu}{2\tilde{\rho}} + \int_{\tilde{\rho}}^{\infty} \mathrm{d}x\ \exp[2K(\tilde{\rho}) - 2K(x)] \\
&\qquad \times \left[2\tilde{\Delta}(x)\tilde{E}x - \frac{\mu\tilde{\Delta}(x)}{x}\right], \\
&\int_{\tilde{\rho}}^{\infty} \mathrm{d}x\ \exp[K(\tilde{\rho}) - K(x)]\left[\frac{1}{x^2} + \frac{\tilde{\Delta}(x)}{x}\right] = \frac{1}{2\tilde{\rho}}.
\end{aligned}
\tag{56}
$$

It is straightforward to solve the above equations for the a_j:

$$a_1 = \mathrm{i}\left(\tilde{E}\tilde{\rho} - \frac{2\,\mu - 1}{2\tilde{\rho}}\right) - \mathrm{i}\int_{\tilde{\rho}}^{\infty} \mathrm{d}x\ \exp[2K(\tilde{\rho}) - 2K(x)] \times\ \tilde{\Delta}(x)\left[2\tilde{E}x - \frac{\mu}{x}\right], \tag{57}$$

$$a_2 = \mathrm{i}\tilde{E}\tilde{\rho} - \mathrm{i}\int_{\tilde{\rho}}^{\infty} \mathrm{d}x\ \exp[2K(\tilde{\rho}) - 2K(x)]\tilde{\Delta}(x)\left[2\tilde{E}x - \frac{\mu}{x}\right], \tag{58}$$

$$a_3 = -\mathrm{i}\left(\tilde{E}\tilde{\rho} - \frac{2\,\mu + 1}{2\tilde{\rho}}\right) + \mathrm{i}\int_{\tilde{\rho}}^{\infty} \mathrm{d}x\ \exp[2K(\tilde{\rho}) - 2K(x)] \times\ \tilde{\Delta}(x)\left[2\tilde{E}x - \frac{\mu}{x}\right], \tag{59}$$

$$a_4 = -\mathrm{i}\tilde{E}\tilde{\rho} + \mathrm{i}\int_{\tilde{\rho}}^{\infty} \mathrm{d}x\ \exp[2K(\tilde{\rho}) - 2K(x)]\tilde{\Delta}(x)\left[2\tilde{E}x - \frac{\mu}{x}\right]. \tag{60}$$

The common integral term in equations (57)–(60) is zero and defines the bound state energy.

A.3. Matching of wave functions

The final step consists in matching the solution for small $\tilde{\rho}$ and large $\tilde{\rho}$ at a distance $\tilde{\rho}_\mathrm{c}$ from the core of the vortex. The condition that this matching is independent of ρ_c determines a unique wave function valid for all $\tilde{\rho}$ and the energy of the bound state.

The solutions for $\tilde{\rho} > \tilde{\rho}_\mathrm{c}$ are now given by $f_j^{\mu}(\tilde{\rho}) = B_j[H_\mu^{(1)}(\tilde{\rho})g_j(\tilde{\rho}) + \mathrm{c.c.}]$, where the coefficients B_j are defined at the beginning of part A.2 of this appendix. They have to be matched at $\tilde{\rho}_\mathrm{c}$ to $f_j^{\mu}(\tilde{\rho})$ given by equation (40) for $\tilde{\rho} < \tilde{\rho}_\mathrm{c}$ with the prefactors defined in part A.1 of this appendix using a similar procedure to reference [26]. The functions g_j were calculated consistently to first order of perturbation and can be written as an exponential, i.e. $g_j(\tilde{\rho}) \propto \exp[-K(\tilde{\rho}) + a_j(\tilde{\rho})]$, which remains correct to first order. To match the wave functions we employ the asymptotic expansions for the Bessel and the Hankel functions given by equations (67) and (68) in appendix B.

There are three factors in f_j depending on $\tilde{\rho}$: (i) the $1/\sqrt{\tilde{\rho}_\mathrm{c}}$-dependence in the Bessel and Hankel functions, (ii) the phase factors of the form $\exp[\mathrm{i}(1 \pm \tilde{E})\tilde{\rho}_\mathrm{c}]$, and (iii) the factors $\exp\{\mathrm{i}[(\mu \pm 1)^2 - 1/4]/[2\tilde{\rho}_\mathrm{c}]\}$. Note that the complex conjugated function for $\tilde{\rho} > \tilde{\rho}_\mathrm{c}$ is also a solution, involving the Hankel function of the second kind. Both solutions are needed to complete the matching.

We explicitly work out the matching for the function f_1^{μ}; the other three functions follow similarly. For $\tilde{\rho} < \tilde{\rho}_\mathrm{c}$ we have

$$f_1^{\mu}(\tilde{\rho}_\mathrm{c}) = A_1 J_{\mu-1}(q_\mathrm{p}\rho) = A_1\sqrt{\frac{2}{\pi(1+\tilde{E})\tilde{\rho}_\mathrm{c}}}\cos\left[(1+\tilde{E})\tilde{\rho}_\mathrm{c} - \frac{\pi(\mu-1)}{2} - \frac{\pi}{4} + \frac{(\mu-1)^2 - \frac{1}{4}}{2(1+\tilde{E})\tilde{\rho}_\mathrm{c}}\right], \tag{61}$$

while for $\tilde{\rho} > \tilde{\rho}_\mathrm{c}$ we obtained

$$f_1^{\mu}(\tilde{\rho}_\mathrm{c}) = [H_\mu^{(1)}(\tilde{\rho}_\mathrm{c})g_1(\tilde{\rho}_\mathrm{c}) + \mathrm{c.c.}] = \frac{1}{2}\sqrt{\frac{2}{\pi\tilde{\rho}_c}}\left\{\exp\left[\mathrm{i}\left(\gamma + \tilde{E}\tilde{\rho}_\mathrm{c} - \frac{(2\mu-1)}{2\tilde{\rho}_\mathrm{c}} + \tilde{\rho}_\mathrm{c} - \frac{\pi\mu}{2} - \frac{\pi}{4} + \frac{\mu^2 - \frac{1}{4}}{2\tilde{\rho}_\mathrm{c}}\right)\right] + \mathrm{c.c.}\right\}\mathrm{e}^{-K(\tilde{\rho}_c)}. \tag{62}$$

In equation (62) the phase γ arises from C, the next two terms in the exponential are due to a_1 and the remainder is consequence of the Hankel function.

From comparing these two expressions it follows that $A_1 = \sqrt{1+\tilde{E}}$ and $\gamma = \pi/2$. As in reference [26] we neglect $\tilde{E}$ in the denominator of the last term in equation (61), because $\tilde{E} \ll 1$, and the factor $\mathrm{e}^{-K(\tilde{\rho}_c)}$ in equation (62). The two expressions are then equivalent and the matching is satisfied for a large interval of $\tilde{\rho}_\mathrm{c}$.

The above hinges on the vanishing of the common integral term in equations (57)–(60), which determines the energy of the bound state, i.e.

$$\int_{\tilde{\rho}_c}^{\infty} \mathrm{d}x\ \exp[2K(\tilde{\rho}) - 2K(x)]\ \tilde{\Delta}(x)\left[2\tilde{E}x - \frac{\mu}{x}\right] = 0. \tag{63}$$

At this point we can take $\tilde{\rho}_\mathrm{c} \to 0$ in the lower integration limit and integrate the first term by parts. This leads to expression (13) for the energy in section 2.

Appendix B. Asymptotic expansion for Bessel and Hankel functions

For large argument the asymptotic expansions for Bessel and Hankel functions are given by [35]

$$J_\nu(z) = \sqrt{\frac{2}{\pi z}}\left[\cos(\omega)\sum_{k=0}^{\infty}(-1)^k\frac{a_{2k}(\nu)}{z^{2k}} - \sin(\omega)\sum_{k=0}^{\infty}(-1)^k\frac{a_{2k+1}(\nu)}{z^{2k+1}}\right], \tag{64}$$

$$H_\nu^{(1)}(z) = \sqrt{\frac{2}{\pi z}}\mathrm{e}^{\mathrm{i}\omega}\sum_{k=0}^{\infty}\mathrm{i}^k\frac{a_k(\nu)}{z^k}, \tag{65}$$

where $\omega = z - \frac{1}{2}\nu\pi - \frac{1}{4}\pi$ and

$$a_k(\nu) = \frac{(4\nu^2 - 1^2)(4\nu^2 - 3^2)\cdots(4\nu^2 - (2k-1)^2)}{k!8^k}. \tag{66}$$

Here we are interested in real positive z. The above expressions can be resummed into the argument of one circular function. Keeping only terms to order $1/z$ in the argument of the circular function we obtain

$$J_\nu(z) = \sqrt{\frac{2}{\pi z}}\cos\left[z - \frac{\pi\nu}{2} - \frac{\pi}{4} + \frac{\nu^2 - \frac{1}{4}}{2z}\right], \tag{67}$$

$$H_\nu^{(1)}(z) = \sqrt{\frac{2}{\pi z}} \exp\left[\mathrm{i}\left(z - \frac{\pi\nu}{2} - \frac{\pi}{4} + \frac{\nu^2 - \frac{1}{4}}{2z}\right)\right]. \tag{68}$$

These equations are exact to this order. CdeGM [26] neglected the $-\frac{1}{4}/(2z)$ in the last term, which is still correct for sufficiently large ν.

Appendix C. Semiclassical approach

The electronic structure at the core of a vortex calculated by CdeGM's can be obtained with semiclassical arguments [5]. In this appendix we present a simple approach for the lowest energy bound states beyond the limitation $|E| \ll E_\mathrm{F}$ used above. Our starting point is again the BdG equations, but to simplify we use a two-component spinor with components $u(\mathbf{r})$ and $v(\mathbf{r})$. The relativistic energy of the bound electron is $E_\mathrm{rel} = vp$, where v is the group velocity. We assume the momentum p can be written as the sum of the radial momentum p_ρ and the angular momentum p_l. Semiclassically, the bound electron is assumed to follow a circular orbit of radius ρ, so that we may neglect p_ρ and $p_l = \mu/\rho$, where μ is the angular momentum about the z-axis.

The BdG equations can then be written as

$$\begin{bmatrix} E - v\mu/\rho + vk_\mathrm{F} & -\Delta(\rho) \\ -\Delta(\rho) & E + v\mu/\rho - vk_\mathrm{F} \end{bmatrix} \begin{pmatrix} u \\ v \end{pmatrix} = 0. \tag{69}$$

For a nontrivial solution the determinant has to be zero

$$E^2 - v^2\left(\frac{\mu}{\rho} - k_\mathrm{F}\right)^2 - \Delta(\rho)^2 = 0, \tag{70}$$

and has roots equal to

$$E_\pm = \pm\sqrt{v^2\left(\frac{\mu}{\rho} - k_\mathrm{F}\right)^2 + \Delta(\rho)^2}. \tag{71}$$

Minimizing the energy with respect to ρ we obtain the radius of the orbit in the confinement potential $\Delta(\rho) = \rho\Delta_\infty/\xi$.

We analyze two special limits, (i) large E_F and (ii) $E_\mathrm{F} = 0$. For large E_F the radius with minimal energy is given approximately by $\rho = \mu/k_\mathrm{F}$ and

$$E_\pm = \pm\frac{\Delta_\infty}{\xi}\frac{\mu}{k_\mathrm{F}} = \pm\mu\frac{\Delta_\infty^2}{vk_\mathrm{F}}, \tag{72}$$

where $\xi = v/\Delta_\infty$. This agrees with the non-relativistic case of CdeGM, where μ is a half-integer. For the relativistic situation μ is an integer and we obtain the correct excited states. For $\mu = 0$ we get $E = 0$ as for the Majorana bound state, but for the wrong reasons, since we neglected the zero point motion for the angular and radial motions.

If $E_\mathrm{F} = 0$ the minimum of the energy is given by $\rho = \sqrt{\mu v\xi/\Delta_\infty} = \sqrt{\mu}\xi = \sqrt{\mu}v/\Delta_\infty$ and the energy is

$$E_\pm = \pm\sqrt{2\,\mu v\Delta_\infty/\xi} = \pm\sqrt{2\,\mu}\Delta_\infty. \tag{73}$$

Hence the radius of the orbit for $\mu = 1$ is ξ, i.e. the coherence length or radius of the vortex, and the excitation energy is $2^{1/2}\Delta_\infty$. This is comparable with numerical calculations by Sau *et al* [5] and Rakhmanov *et al* [10], although our estimate is roughly 50% larger (we neglect quantum fluctuations) for a slightly different model.

ORCID iDs

P Schlottmann https://orcid.org/0000-0001-8979-0405

References

[1] Beenakker C W J 2013 *Annu. Rev. Condens. Matter Phys.* **4** 113
[2] Kitaev A Y 2001 *Phys.-Usp.* **44** 131
[3] Fu L and Kane C L 2008 *Phys. Rev. Lett.* **100** 096407
[4] Fu L and Kane C L 2009 *Phys. Rev. Lett.* **102** 216403
[5] Sau J D, Lutchyn R M, Tewari S and Das Sarma S 2010 *Phys. Rev.* B **82** 094522
[6] Sau J D, Lutchyn R M, Tewari S and Das Sarma S 2010 *Phys. Rev. Lett.* **104** 040502
[7] Mao L and Zhang C 2010 *Phys. Rev.* B **82** 174506
[8] Beenakker C W J 2015 *Rev. Mod. Phys.* **87** 1037
[9] Chiu C-K, Cole W S and Das Sarma S 2016 *Phys. Rev.* B **94** 125304
[10] Rakhmanov A L, Rozhkov A V and Nori F 2011 *Phys. Rev.* B **84** 075141
[11] Akzyanov R S, Rozhkov A V, Rakhmanov A L and Nori F 2014 *Phys. Rev.* B **89** 085409
[12] Hugdal H G, Linder J and Jacobsen S H 2017 *Phys. Rev.* B **95** 235403
[13] Zyuzin A, Alidoust M and Loss D 2016 *Phys. Rev.* B **93** 214502
[14] Bobkova I V and Bobkov A M 2017 *Phys. Rev.* B **96** 224505
[15] Ioselevich P A, Ostrovsky P M and Feigel'man M V 2012 *Phys. Rev.* B **86** 035441
[16] Suzuki S-I, Kawaguchi Y and Tanaka Y 2018 *Phys. Rev.* B **97** 144516
[17] Akzyanov R S, Rakhmanov A L, Rozhkov A V and Nori F 2015 *Phys. Rev.* B **92** 075432
[18] Akzyanov R S, Rakhmanov A L, Rozhkov A V and Nori F 2016 *Phys. Rev.* B **94** 125428
[19] Chamon C, Jackiw R, Nishida Y, Pi S-Y and Santos L 2010 *Phys. Rev.* B **81** 224515
[20] Kraus Y E, Auerbach A, Fertig H A and Simon S H 2009 *Phys. Rev.* B **79** 134515
[21] Hu L-H, Li C, Xu D-H, Zhou Y and Zhang F-C 2016 *Phys. Rev.* B **94** 224501
[22] Durst A C 2016 *Phys. Rev.* B **93** 064514
[23] Sato M, Takahashi Y and Fujimoto S 2009 *Phys. Rev. Lett.* **103** 020401
[24] Khaymovich I M, Kopnin N B, Mel'nikov A S and Shereshevskii I A 2009 *Phys. Rev.* B **79** 224506
[25] Beenakker C W J 2006 *Phys. Rev. Lett.* **97** 067007
[26] Caroli C, de Gennes P G and Matricon J 1964 *Phys. Lett.* **9** 307
[27] Caroli C and Matricon J 1965 *Phys. Kondens. Mater.* **3** 380
[28] Abrikosov A A 1957 *Sov. Phys - ZhETF* **32** 1442
[29] Bardeen J, Kümmel R, Jacobs A E and Tewordt L 1969 *Phys. Rev.* **187** 556
[30] Xu J-P *et al* 2015 *Phys. Rev. Lett.* **114** 017001
[31] Sun H-H *et al* 2016 *Phys. Rev. Lett.* **116** 257003
[32] Wang D *et al* 2018 *Science* **362** 333
[33] Kong L *et al* 2019 *Nat. Phys.* **15** 1181
[34] Chen C, Jiang K, Zhang Y, Liu C, Liu Y, Wang Z and Wang J 2020 *Nat. Phys.* **16** 536
[35] National Institute of Standards and Technology, US Department of Commerce 2010-2020 ed by F W J Olver, D W Lozier, RF Boisvert and C W Clark http://dlmf.nist.gov/10.17